Fundamental Mode Operation of Gunn Devices Above 100 GHz[1]

R. Kamoua, J. R. East, and G. I. Haddad
Center for High Frequency Microelectronics
Solid State Electronics Laboratory
Department of Electrical Engineering and Computer Science
The University of Michigan, Ann Arbor, MI 48109-2122

Abstract

An Ensemble Monte Carlo model capable of predicting the high frequency performance of Gunn devices has been developed. Conventional structures (ohmic cathode) with a linearly graded doping in the active region are predicted to generate rf power at frequencies up to 220 GHz. We have also compared Gunn devices with three types of heterojunction injectors at the cathode : a forward biased triangular barrier, a reverse biased triangular barrier, and a rectangular barrier. In general the optimum frequency for power generation decreases as the injector becomes more efficient in reducing the dead zone. InP Gunn devices resulted in a slightly higher oscillation frequency and output power, however the temperature increase is much larger than GaAs devices.

I INTRODUCTION

The high frequency limit of GaAs Gunn devices in the fundamental mode is generally estimated to be less than 100GHz [1]. This limit is due to intrinsic and extrinsic sources. The intrinsic limitations are related to the physics of the semiconductor and the processes responsible for the Gunn effect. The dominant aspect of Gunn operation at very high frequencies is the fact that the transit time becomes comparable to the nucleation time or the collection time of the accumulation layer. Eventually as the frequency increases, the oscillation period becomes less than the time necessary to nucleate and collect an accumulation layer and the Gunn effect disappears. The short transit time requires a short transit region. At frequencies above 100GHz, the device length should be in the submicron range assuming transit time mode of operation. The susceptance of the Gunn diode increases as the transit region becomes shorter and the frequency is higher. As a

[1]This work was supported by the Center for Space Terahertz Technology under Contract No. NAGW-1334

result, the area required to match to a given load becomes smaller and the output power decreases. A smaller area will also result in a higher series resistance which reduces the circuit efficiency and the power delivered to the load. Independent of the frequency of oscillation, an inactive region required by cold electrons streaming from the cathode to gain enough energy and transfer to the upper valleys exists. As the frequency increases, this inactive region represents a larger fraction of the total transit region. For example in a 1 micron device, the inactive region occupies more than half of the device length. Another important aspect of Gunn device operation is the heat dissipation since most of the input power is not converted to rf power. As the operating temperature increases, the average velocity and the differential negative resistance decrease. This results in a lower oscillation frequency and less output power.

The extrinsic limitations are related to the material growth, fabrication process, mounting and packaging of the device, and the design of a resonant circuit. In order to reduce the series resistance, we need to remove the substrate and optimize the specific contact resistance of the cathode and anode contacts. The mounting and packaging of the Gunn diode are very critical steps because they introduce parasitic resistors, stray capacitors, and lead inductors that can reduce the negative resistance and the output power. The design of a resonant waveguide cavity is difficult at high frequencies because the dimensions of the waveguide are very small. The waveguide is also required to present the diode with a low impedance in order to get useful power.

In this paper, we investigate in more detail the high frequency limitations of GaAs and InP Gunn devices operating in the fundamental mode. We present simulation results using a self consistent Ensemble Monte Carlo model on 1 μm devices with n^+ ohmic contacts as well as heterostructure injectors at the cathode. We consider the effects of the series resistance and the temperature rise on the output power and efficiency versus frequency. We also present simulations on InP devices with n^+ contacts having the same structure as GaAs devices.

II GUNN STRUCTURE

The simulated Gunn structure is shown in Fig. 1. It consists of a $0.1\mu m$ cathode region doped at $2 \times 10^{17} cm^{-3}$, a $0.1\mu m$ heterostructure injector, a $1\mu m$ active region with a linearly graded doping increasing from the cathode toward the anode, and finally a $0.2\mu m$ anode region doped at $2 \times 10^{17} cm^{-3}$. In the case of GaAs diodes, the injector region consists of an AlGaAs layer with an aluminum composition varying from x = x_1 to x = x_2. Three types of injectors are considered: the first 'forward injector' has $x_1 = 0$ and $x_2 = 0.05$, the second.'reverse injector' has $x_1 = 0.05$ and $x_2 = 0$, and the

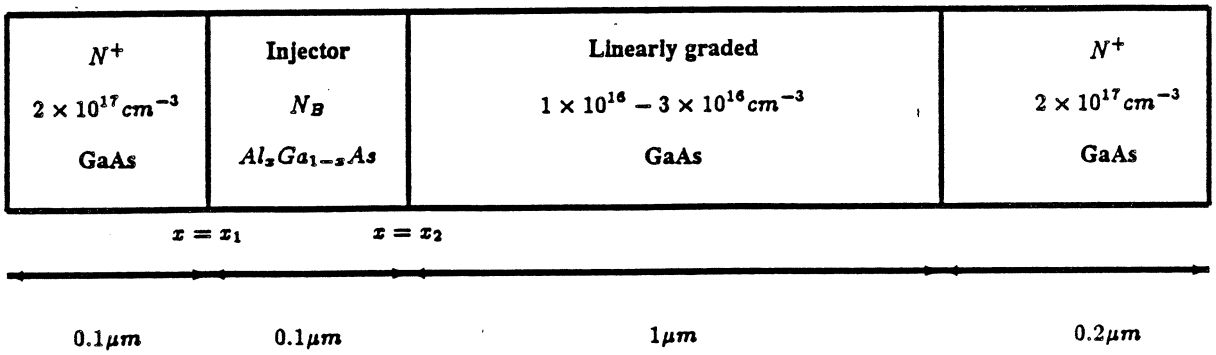

Figure 1: Doping profile of the simulated Gunn structure.

third 'rectangular injector' has $x_1 = 0.05$ and $x_2 = 0.05$. Only n^+ ohmic contacts are considered for the case of InP devices.

III SIMULATION MODEL

The results described in this paper are obtained by using an Ensemble Monte Carlo model which includes three nonparabolic valleys Γ, L, and X. The following scattering mechanisms are included: acoustic, ionized impurity, polar optical phonon, alloy, intervalley, and intravalley scattering. The material parameters are very critical, however values found in the literature vary among different sources. In our simulations, most of the parameters are taken from[2], and [3]. In the case of the heterostructure barrier injector in the cathode region, the material parameters and the effective mass have values that vary with position.

Since the electric field in Gunn structures is nonuniform, the model should be self consistent. In order to update the electric field along the structure, Poisson's equation is solved every 10fs. A more detailed description of the model can be found elsewhere [4]. The device response to an applied voltage is obtained through simulation over many periods (about ten). The resulting particle current density is Fourier analyzed and the fundamental component is used to determine the conductance and susceptance per unit area which are averaged over the last eight r.f. periods. The dc current density is given by:

$$J_{dc} = \frac{1}{2\pi} \int_0^{2\pi} J(\omega t) d(\omega t) \qquad (1)$$

The fundamental component of the current density is expressed as:

$$J_{Fun} = (a_1)cos(\omega t) + (b_1)sin(\omega t) \tag{2}$$

where,

$$a_1 = \frac{2}{T}\int_0^T J(t)cos(\omega t)dt \tag{3}$$

$$b_1 = \frac{2}{T}\int_0^T J(t)sin(\omega t)dt \tag{4}$$

The applied voltage consists of a dc and rf components:

$$V(t) = V_{dc} + V_{rf}sin(\omega t) \tag{5}$$

The device admittance per unit area is :

$$Y_D = J_{Fun}(t)/V(t) = -G_D + jB_D \tag{6}$$

where,

$$G_D = \frac{-b_1}{V_{rf}} \tag{7}$$

$$B_D = \frac{a_1}{V_{rf}} + \frac{\omega\epsilon}{W} \tag{8}$$

In the expression for B_D, the cold capacitance has been added since the displacement current was not taken into account in $J(\omega t)$. The generated rf power is given by:

$$P_{rf}(Gen.) = \frac{1}{2}V_{rf}^2 A G_D, \tag{9}$$

where A is the device area. The rf power across the load R_L is :

$$P_{rf}(R_L) = P_{rf}(Gen)\frac{R_L}{R_L + R_s} \tag{10}$$

where R_s is the series resistance and is expressed as : [5]

$$R_s(f) = \frac{\rho_c + \rho_e L_e}{A} + \frac{\rho_s}{\pi\sigma}[0.5ln(\frac{b}{d}) + \frac{h}{b} + 0.5] \tag{11}$$

where,

ρ_c = specific contact resistance $\Omega.cm^2$ (1×10^7),
ρ_e = epilayer resistivity in $\Omega.cm$ $(\rho_n = 3.7 \times 10^{-4})$,
ρ_s = heat sink resistivity in $\Omega.cm$ (for Gold $\rho_s = 2.35 \times 10^{-6}$),
L_e = length of the contact regions,
σ = skin depth in cm given by : $\sqrt{(\frac{2\rho_s}{\mu\omega})}$,
b = heat sink diameter (0.02 cm),
h = height of the heat sink (0.005 cm),
d = diode diameter in cm.

In order to obtain the output rf power we need to evaluate the device area. The area is determined by satisfying the oscillation condition which is expressed as:

$$X_d + X_L = 0 \tag{12}$$
$$R_d + R_s + R_L = 0 \tag{13}$$

where, $Z_d = R_d + jX_d$ is the total device impedance which can be expressed as :

$$Z_d = \frac{1}{AY_D} = \frac{1}{A}[\frac{-G_D}{G_D^2 + B_D^2} - j\frac{B_D}{G_D^2 + B_D^2}], \tag{14}$$

and $Z_L = R_L + jX_L$ is the load impedance.

From equations (13), (11), and (14), the area can be expressed as:

$$A = [\frac{G_D}{G_D^2 + B_D^2} - \rho_c - \rho_e L_e]/[R_{hs} + R_L] \tag{15}$$

Since the area has to be larger than zero, the specific contact resistance ρ_c has to satisfy the following condition :

$$\rho_c \leq \frac{G_D}{G_D^2 + B_D^2} - \rho_e L_e \tag{16}$$

Substituting the expression for the area in (10), we obtain the rf power delivered to the load R_L :

$$P_{rf}(R_L) = \frac{V_{rf}^2}{2} \frac{[G_D - (\rho_c + \rho_e L_e)(G_D^2 + B_D^2)]^2}{G_D^2 + B_D^2} \frac{R_L}{(R_{hs} + R_L)^2} \tag{17}$$

where,

$$R_{hs} = \frac{\rho_s}{\pi\sigma}[0.5ln(\frac{b}{d}) + \frac{h}{b} + 0.5] \tag{18}$$

III-A THERMAL EFFECTS

Gunn devices at millimeter wave frequencies have very low efficiencies and most of the input power is dissipated as heat. As the device temperature increases, the following may occur [6] :

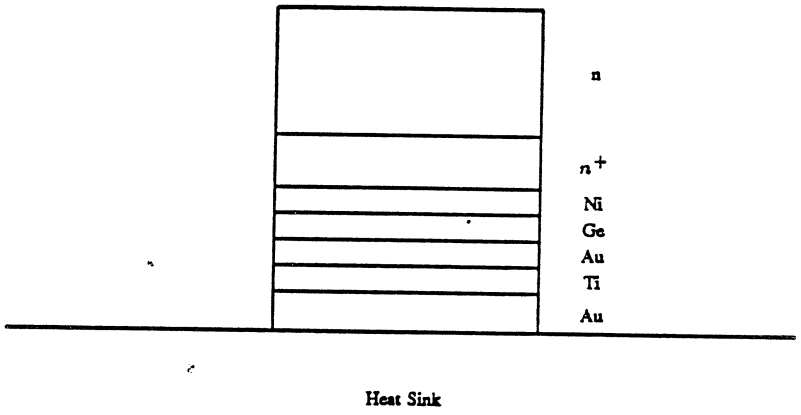

Figure 2: Gunn device mesa structure mounted on a heat sink

- The Arsenic starts to evaporate at 620 $^{\circ}C$,
- The material becomes intrinsic around 450 $^{\circ}C$,
- The alloy contacts melt at 350 $^{\circ}C$,
- The average electron velocity decreases.

From the above considerations it is important to provide a suitable heat sink which should be placed near the anode region where the electric field is highest. The maximum tolerable temperature increase is set to 225 $^{\circ}C$.
Assuming the heat flows toward the heat sink, the maximum temperature occurs at the top of the active region (Fig. 2). In order to determine the maximum temperature in the device, the heat flow equation in each region has to be solved.

$$\frac{d}{dz}(\kappa\frac{dT}{dz}) = -q(z) \tag{19}$$

where,

q = heat generated per unit volume,

κ = thermal conductivity.

Taking into account the temperature dependence of the thermal conductivity, the maximum temperature is expressed as:[7]

$$T_{max} = [T_A + \frac{P}{A}(\frac{d_c}{\kappa_{eff}} + \frac{\sqrt{(\frac{A}{\pi})}}{\kappa_{hs}})]exp[\frac{P}{A}(\frac{W}{4a_1} + \frac{\epsilon}{a_2})] \tag{20}$$

where,

T_A = ambient temperature

P = total dissipated power

A = device area

κ_{eff} = effective thermal conductivity of the contact

κ_{hs} = heat sink thermal conductivity (3.8 $\frac{W}{cm.^oK}$ for copper)

W = active area thickness

ϵ = thickness of the n^+ region

a_1, a_2 defined as :

$$\kappa_a = \frac{a_1}{T} \tag{21}$$

$$\kappa_{n+} = \frac{a_2}{T} \tag{22}$$

where,

κ_a = active region thermal conductivity (150 $\frac{W}{cm.^oK}$ in GaAs),

κ_{n+} = n^+ region thermal conductivity (120 $\frac{W}{cm.^oK}$ in GaAs).

$$d_c = d_{Ni} + d_{Ge} + d_{Au} + d_{Ti} \tag{23}$$

d_{Ni} = thickness of Nickel layer (250 $\mathring{A}$),

d_{Ge} = thickness of germanium layer (325 $\mathring{A}$),

d_{Au} = thickness of Gold layers (2650 $\mathring{A}$),

d_{Ti} = thickness of Titanium layer (100 $\mathring{A}$),

$$\kappa_{eff} = \frac{d_c}{(\frac{d_{Ni}}{\kappa_{Ni}} + \frac{d_{Ge}}{\kappa_{Ge}} + \frac{d_{Au}}{\kappa_{Au}} + \frac{d_{Ti}}{\kappa_{Ti}})} \tag{24}$$

κ_{Ni} = Nickel thermal conductivity (0.9 $\frac{W}{cm^oC}$ at 300 ^oK),

κ_{Ge} = Germanium thermal conductivity (0.6 $\frac{W}{cm^oC}$ at 300 ^oK),

κ_{Au} = Gold thermal conductivity (3.18 $\frac{W}{cm^oC}$ at 300 ^oK),

κ_{Ti} = Titanium thermal conductivity (0.219 $\frac{W}{cm^oC}$ at 300 ^oK).

The total thermal resistance is defined as:

$$R_{Th} = \frac{T_{max} - T_A}{P_{dc}} \tag{25}$$

IV SIMULATION RESULTS

All the results presented below correspond to a Gunn device operated at 300 $^{\circ}K$. The power is obtained by matching the device to a 10 Ω load.

IV-A GAAS DEVICES

IV-A.1 OHMIC INJECTOR CATHODE

In this structure, the cathode region consists of an n^+ layer and no heterojunction barrier is present. Fig. 3a shows the output power and efficiency as a function of frequency for Vdc = 2V and Vrf = 0.4V. The oscillations occur over a wide range of frequencies from 120 to 240 GHz. The efficiency has a peak of 1.5 % at 220 GHz and the power reaches a maximum of 5.3 mW at 180 GHz. The power peaks at a lower frequency than the efficiency because the power is proportional to the efficiency and the area which decreases with frequency.

The maximum power possible at 180 GHz is obtained by varying the rf voltage. Fig. 3b shows the efficiency and power as a function of the rf voltage for Vdc = 2V. A maximum power of 10.5 mW occurs when Vrf = 0.7V with an efficiency of 2.77 % and temperature rise of 68 $^{\circ}K$. A higher output power may be obtained by matching to a smaller load which results in a larger device area and requires more dc power. However the much higher operating temperature results in a lower oscillation frequency and smaller output power because the the 'dead zone' and the carrier velocity are reduced.

The evolution of an accumulation layer is conveyed by plotting the electric field (Fig. 4) across the device at equally spaced time intervals of $\frac{T}{8}$, where T is the period. The variation of the electric field is small in a region near the cathode and is larger toward the anode. Nearly half of the transit region corresponds to a 'dead zone' where most of the electrons did not gain enough energy to transfer to the upper valleys.

The oscillation frequency is frequently estimated from the transit time requirements assuming a drift velocity between 8×10^6 and $1 \times 10^7 \frac{cm}{s}$. For devices in the micron range this is not valid because the transit time is no longer the dominant process in a given cycle. The accumulation layer formation and collection times are comparable to the transit time. A 1 μm device is expected to generate fundamental oscillation at a frequency between 80 GHz and 100 GHz. However, taking into account the overlap in time between the three phases of an accumulation layer (or dipole domain): nucleation,

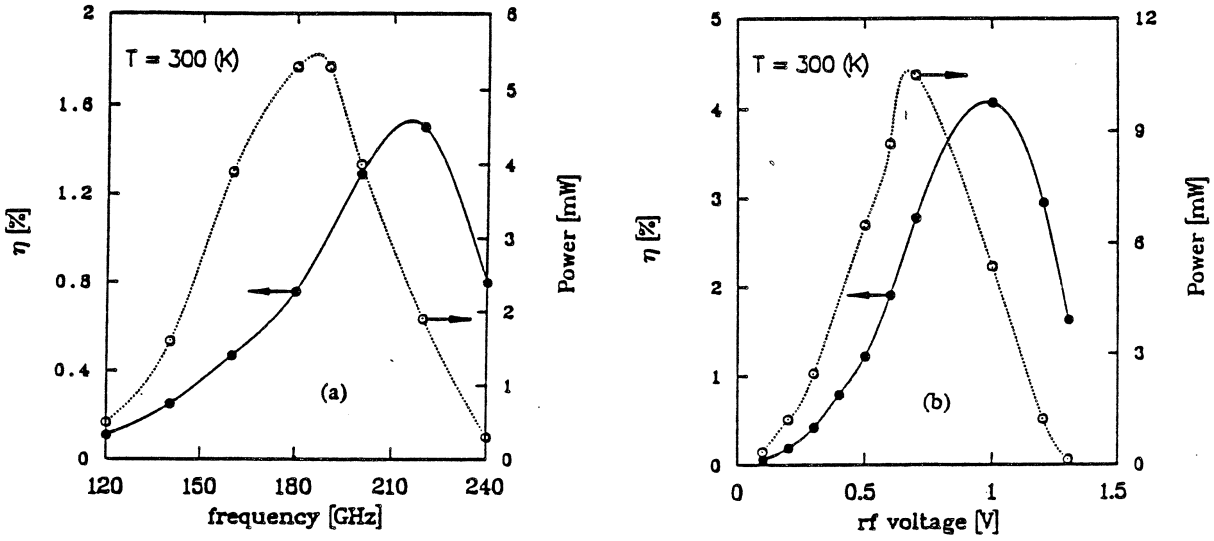

Figure 3: Output power and efficiency for a GaAs diode with ohmic injection, Vdc = 2.0 V: a) versus frequency for Vrf = 0.4 V. b) versus rf voltage for f = 180 GHz.

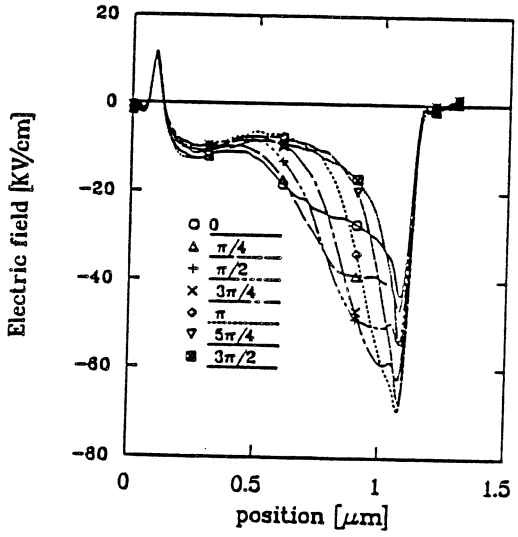

Figure 4: Electric field across the ohmic injector GaAs diode.

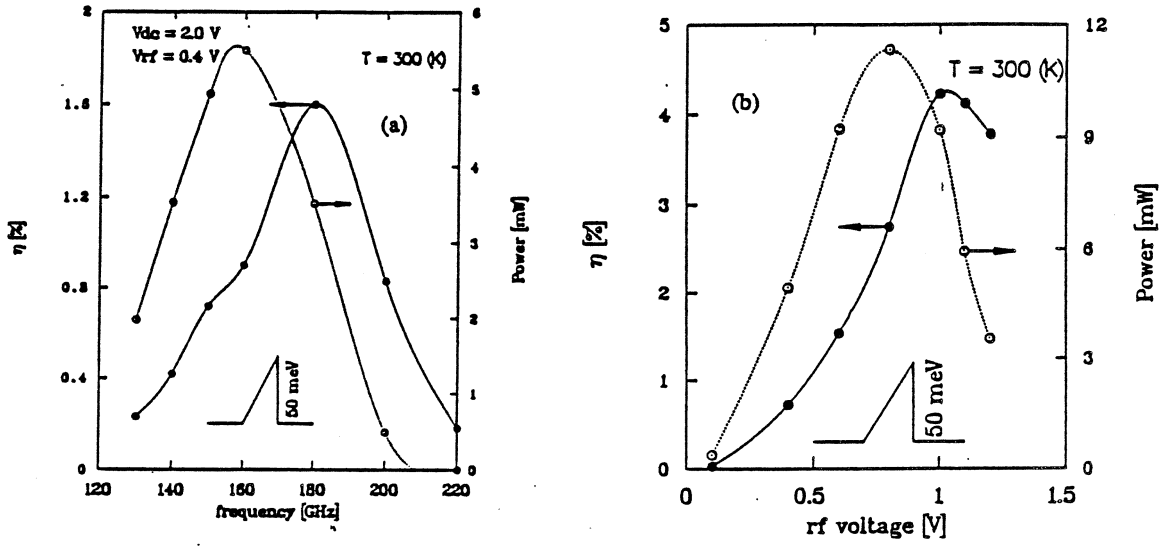

Figure 5: Output power and efficiency for a GaAs diode with a 'forward barrier' injector, Vdc = 2.0 V: a) versus frequency for Vrf = 0.4 V. b) versus rf voltage for f = 150 GHz.

transit, collection and the reduction of the effective transit length due to the dead zone explains the oscillations at frequencies around 180 GHz.

At 180 GHz a 20 μm diameter diode is needed in order to be matched to 10 Ω load. At higher frequencies smaller diodes are required which complicates the bonding process. Increasing the area results in a higher output power but requires matching to a smaller load and mounting the device on a better heat sink.

IV-A.2 'FORWARD INJECTOR' HETEROJUNCTION CATHODE

This structure is similar to the previous one, except a heterojunction triangular barrier injector is added at the end of the n^+ cathode region. Fig. 5a shows the efficiency and output power as a function of frequency for a 50 meV barrier, 0.1 μm wide. The efficiency has a maximum of 1.6 % which occurs at 180 GHz and the power reaches a maximum of 5.5 mW at 160 GHz. In fig. 5b, the effect of changing the rf voltage on the efficiency and power is shown for a frequency of 150 GHz and Vdc = 2 V. When Vrf = 0.8 V, the power reaches a maximum of 11.3 mW with an efficiency of 2.75 %, a temperature rise of 57 $^\circ K$, and a diode diameter of 23 μm. The lower oscillation frequency compared with the previous structure is a result of the 'dead zone' reduction as can be seen in fig. 6 which shows the electric field along the structure. The electric field has a maximum of 45 $\frac{kV}{cm}$ compared with 70 $\frac{kV}{cm}$ in the conventional structure. The lower peak electric field is due to the voltage drop inside the injector region. The addition of

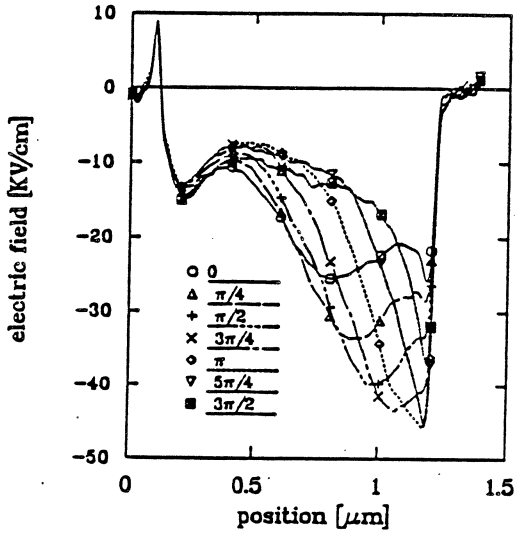

Figure 6: Electric field across the 'forward' barrier injector GaAs diode.

the 'forward injector' has resulted in a shorter 'dead zone' region, smaller temperature rise, lower oscillation frequency, and more power at this frequency.

IV-A.3 'REVERSE INJECTOR' HETEROJUNCTION CATHODE

The barrier injector is similar to the 'forward injector' except that the abrupt side is toward the cathode. Fig. 7a shows the efficiency and output power as a function of frequency. The maximum power is 4 mW and occurs at 150 GHz while the maximum efficiency is 1.2 % at 160 GHz. At 150 GHz and Vdc = 2 V, the maximum power is 5.3 mW when Vrf = 0.6 V (fig. 7b). At this operating point the temperature rise is 41 $^{\circ}K$.

The further reduction in the oscillation frequency compared with the 'forward injector' suggests that the 'reverse barrier' is more effective in reducing the 'dead zone'. This is confirmed by observing the electric field across the structure (fig. 8) which shows clearly a smaller inactive region. We notice also that a domain is formed instead of accumulation layer.

IV-A.4 'RECTANGULAR INJECTOR' HETEROJUNCTION CATHODE

The last cathode injector considered for GaAs Gunn devices is a rectangular barrier 50 meV high. The efficiency and output power as a function of frequency are shown in fig. 9a. The maximum output power is 3 mW at 140 GHz and the maximum efficiency is 0.9 % at 160 GHz. At 140 GHz, the maximum output power possible is 6.7 mW

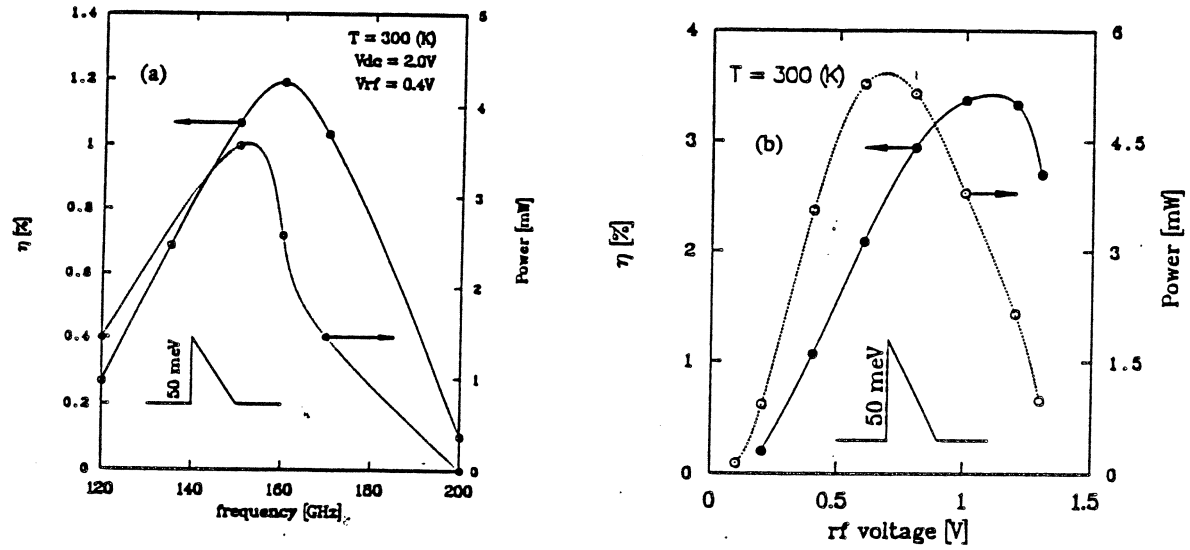

Figure 7: Output power and efficiency for a GaAs diode with a 'reverse' barrier injector, Vdc = 2.0 V: a) versus frequency for Vrf = 0.4 V. b) versus rf voltage for f = 150 GHz.

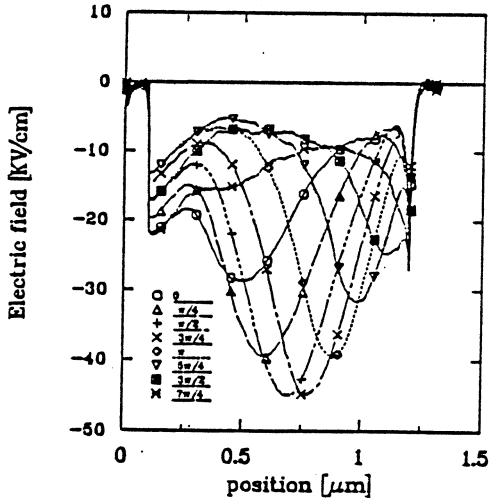

Figure 8: Electric field across the 'reverse' barrier injector GaAs diode.

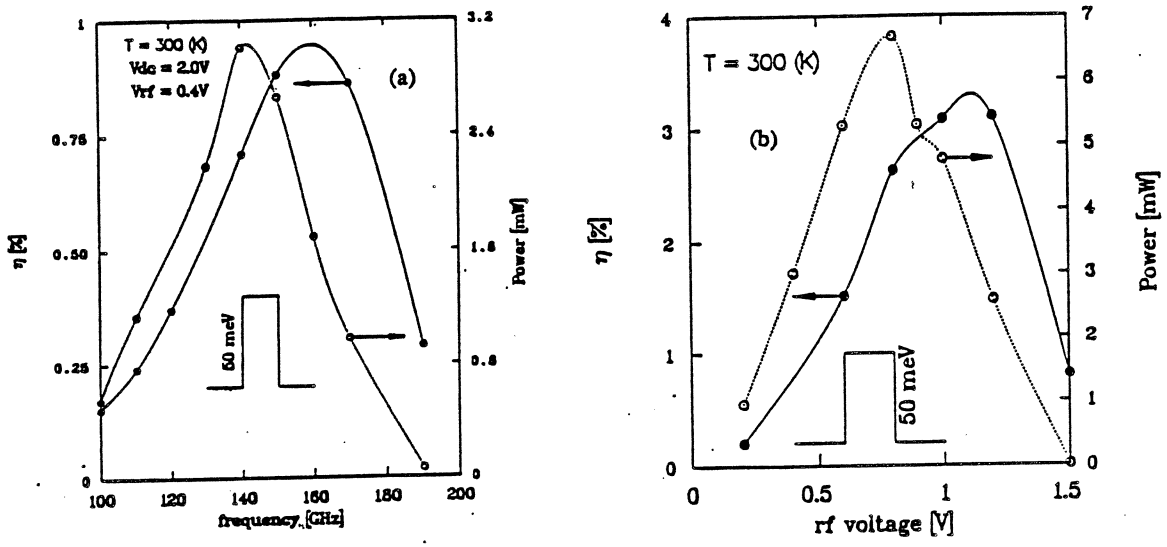

Figure 9: Output power and efficiency for a GaAs diode with a 'rectangular' barrier injector, Vdc = 2.0 V: a) versus frequency for Vrf = 0.4 V. b) versus rf voltage for f = 150 GHz.

for Vrf = 0.8 V with an efficiency of 2.6 %, a temperature rise of 40 $°K$, and a diode diameter of 21 μm (fig. 9b). The electric field is not shown since it is similar to the previous structure except that the variation in the field near the cathode is smaller in the 'rectangular barrier' case.

IV-B InP Gunn DEVICES

InP Gunn devices with a similar structure and doping profile to the ohmic injector GaAs devices are also simulated. Compared with GaAs, InP has a higher energy separation between the Γ and L valley, stronger intervalley scattering mechanisms, and higher electron velocity. As a result a higher dc voltage is needed to observe the Gunn effect. A dc voltage of 6 V is found to result in the best performance. Fig. 10a plots the efficiency and output power as a function of frequency for Vrf = 1.2 . We notice that oscillations extend from 120 GHz to 270 GHz which is slightly higher than in GaAs devices. The maximum efficiency is 1.2 % which occurs at 220 GHz and the maximum output power is 11.2 mW at 200 GHz. Fig. 10b is a plot of the efficiency and power as a function of the rf voltage at 200 GHz. The maximum output power is 15.2 mW at Vrf = 1.5V. At this operating point the diode diameter is 18 μm, the efficiency is 1.35 %, and the temperature rises by 200 $°K$. The electric field is plotted in fig. 11 which shows a smaller 'dead zone' region compared with the similar GaAs structure. The peak electric

field of 170 $\frac{KV}{cm}$ near the anode is much larger than inside the GaAs device which may lead to electronic failures.

It has been reported [8] that InP devices with a current limiting contact such as a Schottky barrier result in a better performance than n^+ ohmic cathode devices. This can be explained by the fact that a current limiting contact will result in a smaller dc power, peak electric field, and maximum temperature rise. Although the dc power is reduced, the actual output rf power is increased because Gunn devices operate much better at low temperatures.

V CONCLUSIONS

We have performed computer simulations on GaAs and InP Gunn devices. Structures with the conventional n^+ ohmic injector resulted in the highest oscillation frequency. Three types of injectors in the cathode region have been considered. The 'reverse barrier' and the 'rectangular barrier' are more effective in reducing the dead zone than the 'forward injector' but generate less power. It is possible to decrease the 'dead zone' even further by increasing the barrier height. However a point is reached where the fraction of electrons in the upper valleys is large in most of the device. This results in a smaller variation of the current density during one cycle and degrades the performance.

The 'dead zone' is considered to be a parasitic positive series resistance and as such its reduction is advantageous. However according to the results presented in this paper this inactive region is not necessarily undesirable. In order to reduce the dead zone, we need to use a cathode injector different from the ohmic injector. This non-ohmic injector, while reducing the 'dead zone', introduces itself an additional series resistance. Furthermore if we assume that the dead zone can be eliminated, then to achieve oscillations around 200 GHz requires a half micron device which has a larger cold capacitance than the $1\mu m$ structure considered above.

InP devices are capable of generating more power and oscillating at higher frequencies than GaAs devices. However as a result of the larger dc power requirements, the temperature rise is much larger than inside GaAs devices. This requires the use of better heat sinks such as diamond or reducing the device area wich results in smaller output power.

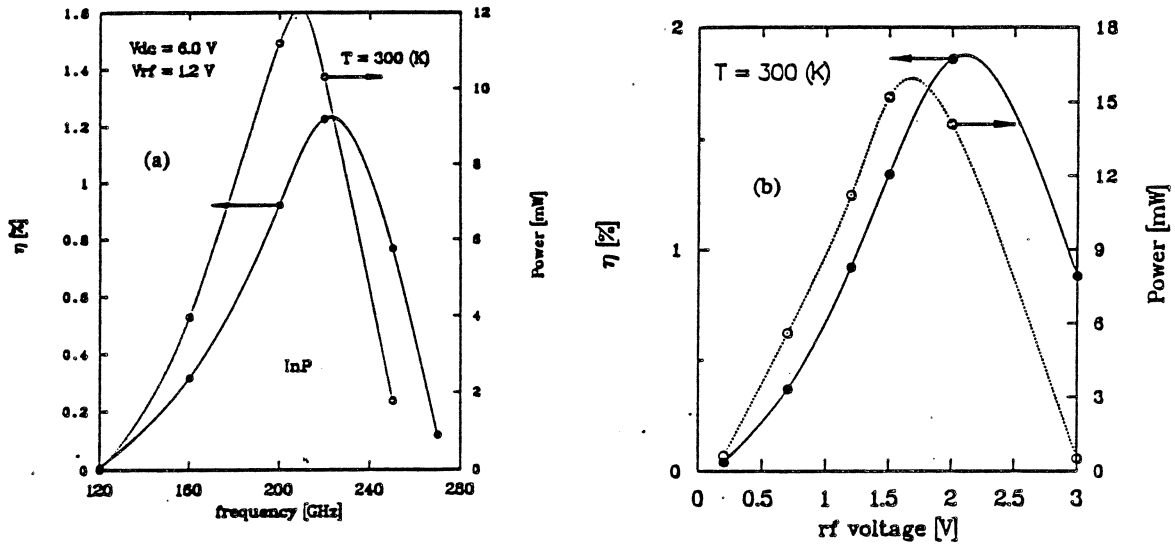

Figure 10: Output power and efficiency for an InP diode with ohmic cathode, Vdc = 6.0 V: a) versus frequency for Vrf = 1.2 V. b) versus rf voltage for f = 200 GHz.

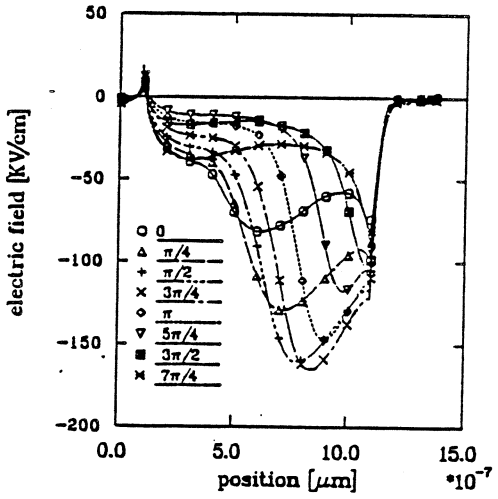

Figure 11: Electric field across the InP Gunn diode.

References

[1] M. J. Lazarus, F. R. Pantoja, S. Novak, and M. G. Somekh, Electron. lett., **17**, No. 20, pp. 739 (1981).

[2] S. Adachi, J. Appl. Phys., **58**(3), pp. 3825 (1987).

[3] M. A. Littlejohn, J. Appl. Phys., **48**, No. 11, pp. 4587 (1977).

[4] R. Kamoua, J. R. East, and G. I. Haddad, J. Appl. Phys., **68**(3), pp. 1114 (1990).

[5] L. E. Dickens, IEEE trans. on M.T.T., Vol. MTT-15, No. 2, pp. 101-109, February. 1967.

[6] B. G. Bosch, R. W. H. Engelmann, Gunn Effect Electronics, (Wiley & Sons, New York, 1974).

[7] A. S. Clorfeine, The Microwave Journal, March 1968, pp. 93.

[8] J. D. Crowley, J. J. Sowers, B. A. Janis, and F. B. Fank, Electron. lett., **16**, No. 18, pp. 705 (1980).